ACS Catalysis

Research Article

pubs.acs.org/acscatalysis

Role of Acidic Proton in the Decomposition of NO over Dimeric Cu(I) Active Sites in Cu-ZSM-5 Catalyst: A QM/MM Study

P. K. Sajith,[†] Yoshihito Shiota,[†] and Kazunari Yoshizawa*[,†,‡]

[†]Institute for Materials Chemistry and Engineering and International Research Center for Molecular Systems, Kyushu University, Fukuoka 819-0395, Japan

[‡]Elements Strategy Initiative for Catalysts & Batteries, Kyoto University, Katsura, Kyoto 615-8520, Japan

Supporting Information

ABSTRACT: The influence of protons on the mechanism of the direct decomposition of NO over adjacent dimeric Cu(I) active sites in zeolite is theoretically investigated by using ONIOM (QM/MM) calculations with two dicopper model systems **1T** and **2T**, where the Cu(I) atoms are separated by one and two SiO_4 tetrahedra, respectively. The reaction proceeds through the formation of N_2O as a reaction intermediate and further its decomposition into oxygen and nitrogen. The present study shows that the presence of proton plays an important role in the production of N_2O from two NO molecules. In the proton-free mechanism, this process requires a large activation barrier of 56.3 and 55.3 kcal/mol on **1T** and **2T**, respectively, while the inclusion of protons reduces it to 31.4 and 17.3 kcal/mol. The significant decrease in the activation barrier is due to the strengthening of the N−N bond of the formed NO dimer upon protonation, which facilitates the formation of N_2O. On the other hand, the presence of protons disfavors the decomposition of N_2O and needs an activation barrier of 6−9 kcal/mol higher than that of the corresponding reaction in the absence of protons. The stable intermediate Cu−OH^+−Cu formed in the proton-assisted mechanism is responsible for the larger activation energy for N_2O decomposition. The proton-assisted NO decomposition mechanism is in agreement with the experimental observation that the decomposition of N_2O as well as O_2 desorption are the governing reaction steps in the decomposition of NO. The present study explains the role of the Cu−O−Cu species in the NO decomposition reaction. The results disclosed herein will also pave a way to understanding the mechanism of the reductive N−N coupling of NO molecules catalyzed by metalloenzymes and transition-metal catalysts.

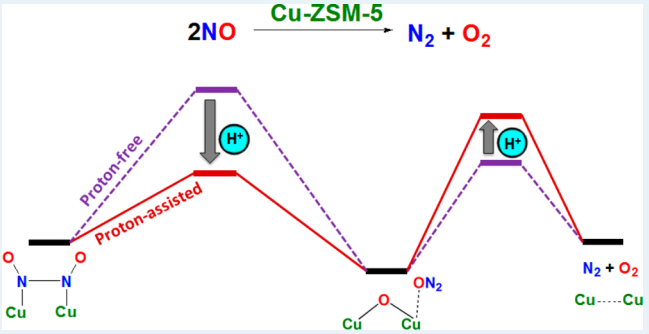

KEYWORDS: *NO decomposition, QM/MM calculation, reaction mechanism, zeolite, Cu-ZSM-5, protonation, metal active site*

INTRODUCTION

The direct catalytic conversion of nitric oxide to nitrogen and oxygen ($2NO \rightarrow N_2 + O_2$)[1] has been an active field of research because of the harmful effects of NO on the environment. Copper exchanged zeolites, in particular Cu-ZSM-5, exhibit the fascinating ability to decompose NO at moderate temperatures between 673 and 773 K.[2−5] Cu-ZSM-5 has also drawn much attention in the selective catalytic reduction of NO with hydrocarbons in the presence of oxygen.[6] Even though the practical applications of Cu-ZSM-5 are limited due to low hydrothermal stability of the material,[1,7] systematic studies to understand the mechanism of Cu-ZSM-5 mediated NO decomposition are essential for the fine-tuning of the activity of catalysts as well as for the design of novel materials with enhanced activity.

The most active site for NO decomposition, whether it is a single Cu ion or pairs of Cu ions, is still controversial, and so far no consensus has been reached.[8−12] The existence of copper atoms with different oxidation states (+1 and +2) in Cu-ZSM-5 is well established in several experimental and theoretical studies.[13,14] Experimental studies revealed that the turn over frequency (TOF) of the NO decomposition reaction is directly related with the Cu loading of the zeolite.[2,3] A plot of TOF versus copper content yields a sigmoidal curve with high activity of NO decomposition nearly at the exchange capacity of the ZSM-5 catalyst.[3,15−17] There is also a linear dependence between TOF and the aluminum framework content of ZSM-5.[15−17] These factors led to the conclusion that dinuclear Cu^+ species may be active for the NO decomposition reaction.[5] Also, the presence of mono-(μ-oxo)-dicopper species is recognized on the basis of UV−vis, EXAFS, and FT-IR studies.[18−22] Schoonheydt and co-workers proposed bis(μ-oxo)dicopper as an active species for Cu-ZSM-5 catalysis based on UV−visible spectroscopic studies.[10] Further, EPR studies strengthened these arguments, and they showed that higher activity of Cu-ZSM-5 for NO and N_2O decomposition compared to other Cu-zeolites is strongly dependent on the amount of bis(μ-oxo)dicopper core present in Cu-ZSM-5.[10,23]

Received: November 20, 2013
Revised: May 8, 2014
Published: May 15, 2014

Da Costa et al. proposed that the formation of unstable Cu dimers is responsible for the higher TOF of NO on Cu-ZSM-5 observed at greater Cu/Al ratios.[24] Using a combined quantum mechanics/interatomic potential function technique (QM-Pot)[25] with the B3LYP[26] method, Sauer and co-workers identified the existence of various types of Cu^+ pairs in ZSM-5.[27] On the other hand, evidence for the presence of isolated Cu ions is also reported by several experimental groups.[13,28−32] Lamberti et al. investigated the local environment of Cu ions in Cu-ZSM-5 by combined use of EXAFS, IR, and photoluminescence UV−vis spectroscopic studies and suggested that Cu atoms exist as isolated Cu^+ ions with two different environments depending upon the coordinative unsaturation of the copper ion.[29] On the basis of photoluminescence, X-ray absorption fine structure, and IR measurements, Itadani et al. ruled out the possibility of dinuclear Cu models as an active site for N_2 adsorption and proposed a three coordinated monomeric Cu^+ ion model.[30,33] Anpo et al. observed the coexistence of both copper dimeric species and isolated Cu^+ ions with the help of photoluminescence spectroscopic studies.[34] All these findings emphasize that the isolated Cu ions as well as pairs of Cu ions are present in Cu-ZSM-5, and the nature of such active sites significantly depends on the extent of Cu loading.[12,35,36] The existence of copper clusters in over-exchanged Cu-ZSM-5 is generally accepted, particularly when the Cu/Al ratio exceeds 0.5.[9] Thus, it is important to consider dinuclear Cu active sites also while discussing the reaction mechanism hosted by Cu-ZSM-5.[37,38] Some recent studies that support the presence of the dinuclear copper active sites are given here. On the basis of DFT calculations, Yumura and co-workers investigated the influence of spatial constraints from the zeolite framework on the reaction intermediates formed during dioxygen activation using dicopper models in the 10-membered ring of the ZSM-5 framework.[39] They found that oxygen activation is highly dependent on the binding modes of dioxygen as well as the distance between Cu pairs. Solomon and co-workers assigned the dinuclear $[Cu_2O]^{2+}$ core as an active site for the study of selective oxidation of methane to methanol over Cu-ZSM-5.[40] On the basis of theoretical calculations, Pidko et al. demonstrated that oxygenated and hydroxylated cationic metal complexes in high silica ZSM-5 tend to form dinuclear multiple charged cationic clusters through self-organization.[41]

The mechanism of NO dissociation is believed to proceed through the formation of the intermediate N_2O ($2NO \rightarrow N_2O + [O]$) at the Cu active site, which leaves the copper-oxo center.[21,42−44] The copper-oxo center facilitates the further decomposition of N_2O into oxygen and nitrogen, thus restoring the initial active site.[43,45] Significant theoretical studies have been devoted to this issue, and most of these studies considered the active site as isolated Cu^+ ions or CuO species in the zeolite framework.[45−49] Most of the theoretical studies suggested O-down coordinated Cu−ON as the starting species for the NO decomposition reaction.[45,50] By means of quantum chemical calculations, Schneider and co-workers reported that the single-step, concerted, direct decomposition of NO to N_2 and O_2 over a Cu ion active site in zeolites is forbidden by orbital symmetry, and the reaction occurs via complex multistep decomposition processes.[48,51] The same authors also analyzed reaction pathways of the above reaction with isolated Cu ions in the zeolite model as an active species, and their study showed that the key intermediates in the catalytic cycle are the metastable species like CuON, $CuON_2$, and CuO_2 in the zeolite framework.[45] Tajima et al. demonstrated that the strong covalent π(d-p) bonding between adsorbed molecules and Cu is responsible for the enhanced catalytic activity of Cu^+ in zeolites compared to isolated Cu^+ ion.[52] Sodupe and co-workers considered CuO as an active site for NO decomposition wherein the adsorption of one and two NO's on the active site leads to the formation of $CuNO_2$ and $Cu(NO_2)(NO)$ species, respectively, which on decomposition regenerate an active site along with the products N_2 and O_2.[53] Izquierdo et al. proposed that an intermediate of the type Cu−η^2-NO, which is in dynamic equilibrium with Cu−ON and Cu−NO, plays an important role in the NO decomposition reaction.[54] Recently, Morpurgo et al. considered a pair of Cu^+ ions at the opposite side of the 10-membered ring of Cu-ZSM-5 as an active site for NO decomposition, and they concluded that the dicopper mechanism is not favored compared to the mechanism that occurs at the isolated Cu^+ active site.[55] Zakharov et al. proposed copper oxide chains (−O−Cu−O−Cu) as an active site for the decomposition of the NO dimer through the formation of an intermediate ONNO on the terminal Cu^+ ion.[56] Although their model system contains two Cu ions, only one Cu is directly involved in the decomposition reaction. To the best of our knowledge, no theoretical studies have been reported on the mechanism of the NO decomposition reaction hosting adjacent bare dicopper units (Cu−Cu) as an active site in the Cu-ZSM-5 framework. In view of all these facts, along with the observation that most of the nitric oxide reductase (NOR) type reactions ($2NO + 2H^+ + 2e \rightarrow N_2O + H_2O$) catalyzed by metalloenzyme as well as transition metals mediated by dinuclear anchoring units, we were motivated to propose a dinuclear Cu model for the decomposition of NO for the present study. The reaction sequence proposed by Kuroda and Iwamoto is shown in Scheme 1.[57]

Scheme 1. Possible Mechanism for the NO Decomposition Reaction[57]

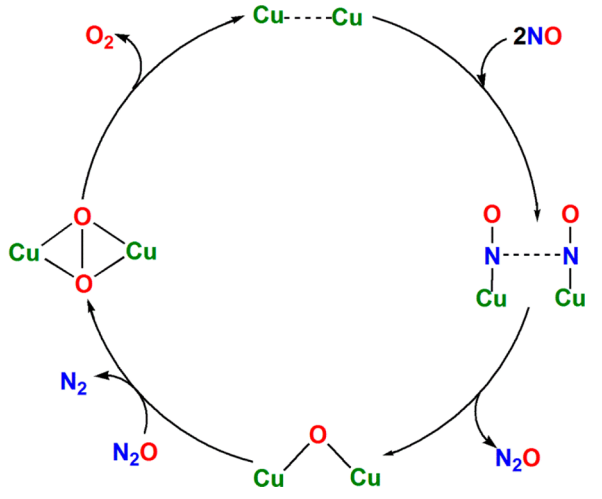

Arikawa and co-workers recently reported that protonation plays a key role for the reduction of NO to N_2O at the dinuclear Ru sites of $[\{TpRu(NO)\}_2(\mu\text{-Cl})(\mu\text{-pz})](BF_4)_2$ complexes (where Tp = hydrotris(pyrazolyl)borate).[58,59] These findings emphasize that protonation facilitates N_2O formation by the N−N coupling of two NO molecules.[60] In zeolites, the Brønsted acid sites catalyze many chemical

dx.doi.org/10.1021/cs500223z | ACS Catal. 2014, 4, 2075−2085

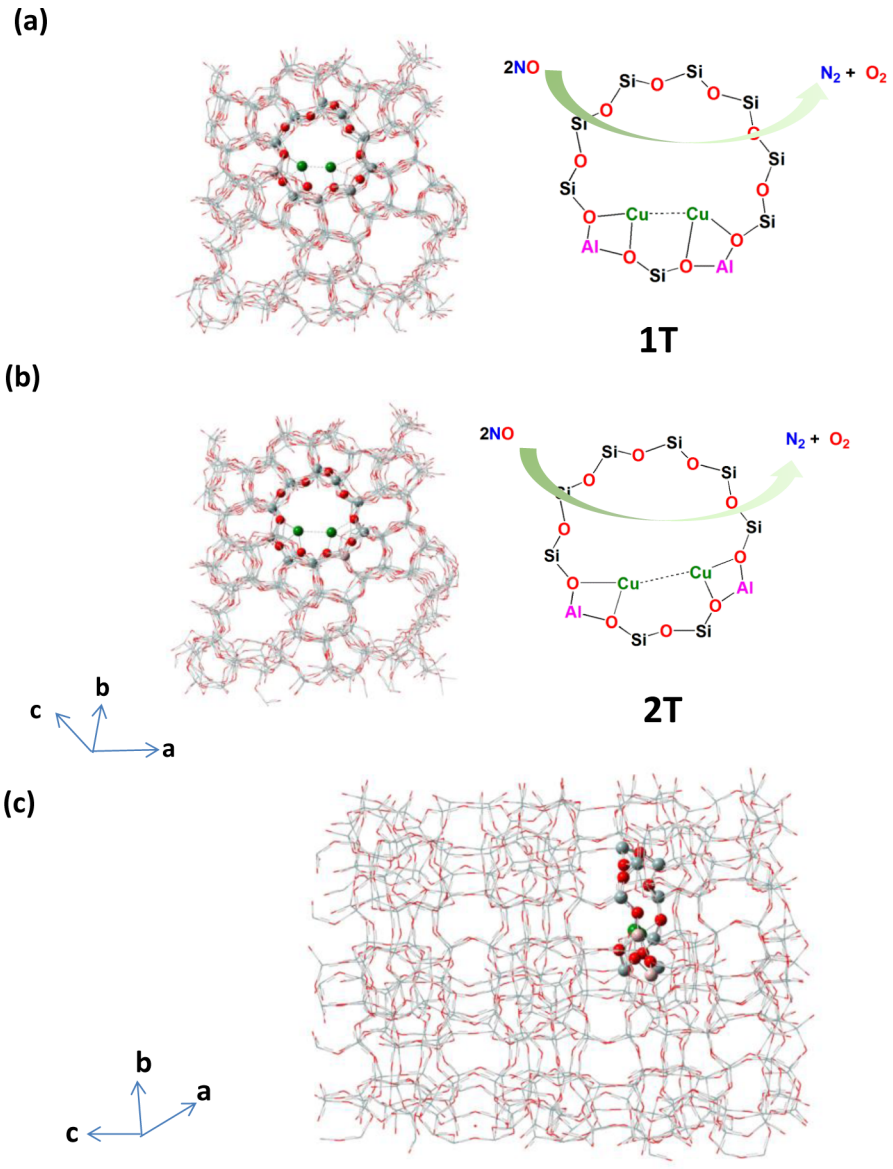

Figure 1. Schematic representation of the zeolite structures employed in the present study. The 10T cluster model in the intersection of straight and zigzag channel with a pair of Cu atoms along with the aluminum T-sites are treated as high-level calculations in the ONIOM method. The QM region is represented by balls and sticks, and the corresponding structures are indicated in the right-hand side of the figure. (a and b) The second and third nearest neighboring aluminum sites along with the two Cu(I) atoms in the 10-membered ring, respectively. (c) The framework of zeolite projected along the c direction.

reactions such as the conversion of hydrocarbons, dehydrogenation reactions, hydrogen exchange, etc.[61,62] However, the involvement of the Brønsted acid sites in the NO decomposition reaction is hardly discussed in the literature.[63] The present study will focus on the influence of a proton on the mechanistic pathways of the direct decomposition of NO mediated by dicopper units in Cu-ZSM-5. We performed a QM/MM study using a model system in which copper ions bound to an aluminum pair are separated by one and two SiO_4 tetrahedra (T) units in the 10-membered ring of the zeolite framework. First, we will explain the proton-free NO decomposition mechanism, and this will be compared using the proton-assisted mechanism.

METHODOLOGY

Computational Methods. Since porous effects of the zeolite framework play an important role in the reactions mediated by zeolites, cluster-model calculations using a quantum chemical method are not sufficient to understand such reactions. The quantum mechanical/molecular mechanical (QM/MM) method, where the reaction field treated with quantum mechanics and the extended framework of zeolite treated with molecular mechanics, was found to be appropriate for describing zeolite-mediated chemical reactions.[64] In this regard, the two-layered integrated molecular orbital + molecular mechanics (ONIOM) method[65,66] is a current state of the art for modeling such reactions.[67−70] Thus, we performed all the calculations using the ONIOM (QM/MM) approach implemented in the Gaussian 09 program.[71] The substrates, two Cu atoms, a proton, and the 10-membered ring containing active

dx.doi.org/10.1021/cs500223z | ACS Catal. 2014, 4, 2075−2085

sites were treated with a high-level quantum mechanical (QM) method, and the remaining extended zeolite framework was treated with a low-level molecular mechanics (MM) method. The number of atoms in the QM layer varied from 42 to 49, which also contained link hydrogen atoms. The electrostatic interaction between the QM and the MM layers was treated by using the electronic embedding approach.[72] This allowed us to incorporate the columbic interaction of the extended zeolite framework to the reacting species. The B3LYP functional[26,73] was used for the high level QM region with the 6-31G(d,p) basis set for all atoms except Cu. For Cu, the Wachters−Hay all electron basis set was used.[74,75] The combined basis set is denoted as BS. The closed-shell singlet, open-shell singlet, and triplet spin states were considered in the present study. The universal force field (UFF) approach[76] with no charge given to atoms was employed for the low-level MM calculations. The UFF method has been widely used to describe the confinement effects of the extended zeolite framework to various guest molecules.[70,77−80] On the basis of experimental details as a benchmark, Limtrakul and co-workers suggested that the UFF method is appropriate for a low-level methodology in the ONIOM calculation for the realistic modeling of the zeolite framework.[79,81,82] The UFF method is also recommended in several studies because it accounts for the van der Waals contribution nicely, which helps to understand the adsorption and desorption of small molecules in zeolites.[68,83−85]

The total energy of the system within the framework of the ONIOM method can be expressed by using eq 1:

$$E^{\text{total}} = E^{\text{QM}}(\text{B3LYP}) + E^{\text{MM}}(\text{UFF}) - E^{\text{QM}}(\text{UFF}) \quad (1)$$

We examined possible reaction pathways on the QM/MM potential energy surfaces. Since DFT energies of the QM region directly reflect the energetics of the reaction, we considered the E^{QM}(B3LYP) values only.[64] All the transition states were characterized by one imaginary frequency and their relative motion. In addition, intrinsic reaction coordinate (IRC) calculations were performed to clarify the connectivity between some of the transition states and its corresponding minima. In order to get accurate energy values, single-point energy calculations were further done at the ONIOM(B3LYP/6-311++G(d,p):UFF) level of theory. All the reported energy and spin density values correspond to the calculations at the ONIOM(B3LYP/6-311++G(d,p):UFF)//ONIOM(B3LYP/BS:UFF) level, unless otherwise noted. To assess the validity of the energetic parameters obtained by using the B3LYP functional, single-point energy calculations were also performed at the ONIOM (B3LYP*/BS:UFF)[86,87] and the ONIOM (TPSSh/BS:UFF) levels[88] of theory using the geometries obtained at the ONIOM (B3LYP/BS:UFF) method. The hybrid B3LYP* functional is an improved version of B3LYP for the calculation of accurate spin-state splitting. The B3LYP* contains 15% Hartree−Fock exchange rather than 20% in the B3LYP functional, whereas the TPSSh is a hybrid meta functional with 10% exchange.

Models for Cu-ZSM-5. The ZSM-5 zeolite system was modeled by using the MFI framework retrieved from the zeolite database[89] consisting of 502-tetrahedron (T) sites (502T = 500 Si + 2Al) containing three straight and zigzag channels formed by 10-membered rings. The optimized geometries of the models are shown in Figure 1. As shown here, confinement effects of the zeolite structures are included in the present model. Two of the silicon atoms from a 10-membered ring, located at the open space in the intersection of the zigzag and straight gateways of the zeolite framework, are substituted by aluminum atoms, and the charge is balanced by Cu^+ ions. This is shown as a ball-and-stick representation in Figure 1. This model was used as a reliable and computationally efficient approach for the studies of activation of small molecules on the zeolite confinement.[39] Zeolite-mediated reactions can reasonably occur in the channel intersection of the zigzag and straight gateways because of the large vacant space available which allows free movement of the reactant molecules. The choice of the 10-membered ring for the QM region allows us to understand the possible interaction of the reacting species, particularly the proton on the oxygen atom of the zeolite framework. The 10-membered ring containing aluminum tetrahedra has been employed as a model system to understand the mechanism of ZSM-5 mediated chemical reactions as well as to study adsorption properties of guest molecules on ZSM-5 by several research groups.[70,80,90,91] The Cu(I) incorporated aluminum pairs separated by one and two SiO_4 tetrahedra (T) were considered in the present models, which are designated as **1T** and **2T**, respectively. For the model systems, the closed-shell singlet state is found to be more stable than the triplet state by 34.9 kcal/mol. Also, **1T** is slightly stable than **2T** by 0.8 kcal/mol. Calculated distances between the Cu−Cu pair are 2.594 and 3.064 Å respectively for **1T** and **2T** models. This is in line with the experimentally reported Cu−Cu distances, which fall in the range of 2.47−3.13 Å.[37,39,92,93]

RESULTS AND DISCUSSION

The proposed mechanism based on our calculations for the proton-free NO decomposition mechanism over the dicopper active site is shown in the following sequence of steps.

$$\text{Cu−Cu} + 2\text{NO} \rightarrow \text{Cu−N(O)−N(O)−Cu} \quad (2)$$

$$\text{Cu−N(O)−N(O)−Cu} \rightarrow \text{Cu}(\text{N}_2\text{O})\text{−O−Cu} \quad (3)$$

$$\text{Cu}(\text{N}_2\text{O})\text{−O−Cu} \rightarrow \text{Cu−O−Cu}(\text{ON}_2) \quad (4)$$

$$\text{Cu−O−Cu}(\text{ON}_2) \rightarrow \text{Cu−O}_2\text{−Cu} + \text{N}_2 \quad (5)$$

$$\text{Cu−O}_2\text{−Cu} \rightarrow \text{Cu−Cu} + \text{O}_2 \quad (6)$$

As given in eq 2, the reaction is initiated by the adsorption of two NO molecules on the different Cu active sites. The formation of N_2O on the Cu active sites is given by eq 3. Equations 4 and 5 describe further reassociation of N_2O on the Cu−O−Cu species, thus producing Cu−O_2−Cu and N_2. The regeneration of the active Cu−Cu species by O_2 desorption is expressed by using eq 6. The proton-assisted mechanism can be represented by the following equations:

$$\text{Cu−Cu} + 2\text{NO} + \text{H}^+ \rightarrow \text{Cu−N(O)−N(OH}^+\text{)−Cu} \quad (7)$$

$$\text{Cu−N(O)−N(OH}^+\text{)−Cu} \rightarrow \text{Cu}(\text{N}_2\text{O})\text{−OH}^+\text{−Cu} \quad (8)$$

$$\text{Cu}(\text{N}_2\text{O})\text{−OH}^+\text{−Cu} \rightarrow \text{Cu−OH}^+\text{−Cu}(\text{ON}_2) \quad (9)$$

$$\text{Cu−OH}^+\text{−Cu}(\text{ON}_2) \rightarrow \text{Cu−O}_2(\text{H}^+)\text{−Cu} + \text{N}_2 \quad (10)$$

$$\text{Cu−O}_2(\text{H}^+)\text{−Cu} + 2\text{NO} \rightarrow \text{Cu−O}_2(\text{H}^+)\text{−Cu(NO)}_2 \quad (11)$$

$$\text{Cu−O}_2(\text{H}^+)\text{−Cu(NO)}_2 \rightarrow \text{Cu−Cu(NO)}_2\text{H}^+ + \text{O}_2 \quad (12)$$

dx.doi.org/10.1021/cs500223z | ACS Catal. 2014, 4, 2075−2085

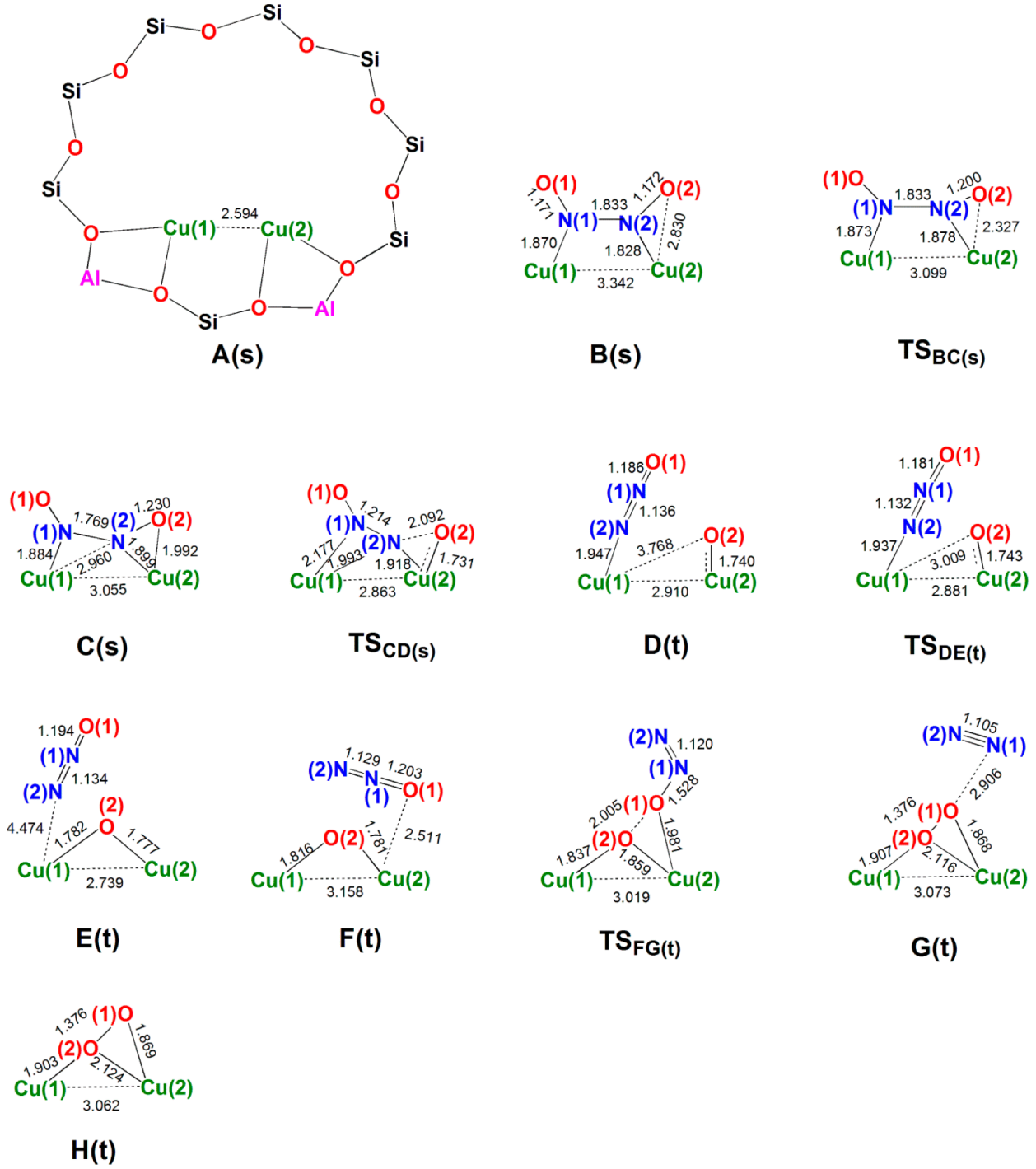

Figure 2. Structures of intermediate and transition state involved in the proton-free NO decomposition mechanism. The spin state for all the structures is shown in parentheses. s is for closed-shell singlet, and t is for triplet state. The 10-membered zeolite framework is omitted for all the structures except for **A(s)**. Bond distances in Å are also given.

$$Cu{-}Cu(NO)_2H^+ \rightarrow Cu{-}N(O)N(OH^+){-}Cu \quad (13)$$

In the presence of a proton, the adsorption of two NO molecules on the different Cu active sites leads to the formation of Cu−N(O)−N(OH$^+$)−Cu. This is shown in eq 7. As described in eq 8, the Cu−N(O)−N(OH$^+$)−Cu species further produces a N_2O molecule, which is weakly bound to one of the Cu active sites. Equation 9 describes the reassociation of N_2O with oxygen as a coordinating atom, resulting in the formation of Cu−OH$^+$−Cu(ON_2). Oxygen transfer from ON_2 to Cu−OH$^+$−Cu yields an N_2 molecule, as given in eq 10. Further coordination of the two NO molecules on one of the Cu active sites can abstract a proton, which is represented by eqs 11 and 12. This leads to the formation of an O_2 molecule. The Cu−$Cu(NO)_2H^+$ species formed will isomerize to the initial complex, described in eq 13. The overall reaction is the formation of N_2 and O_2 from two NO molecules and the sum of all the reactions will be the catalytic cycle for the NO decomposition reaction. In the following section, we describe

dx.doi.org/10.1021/cs500223z | ACS Catal. 2014, 4, 2075−2085

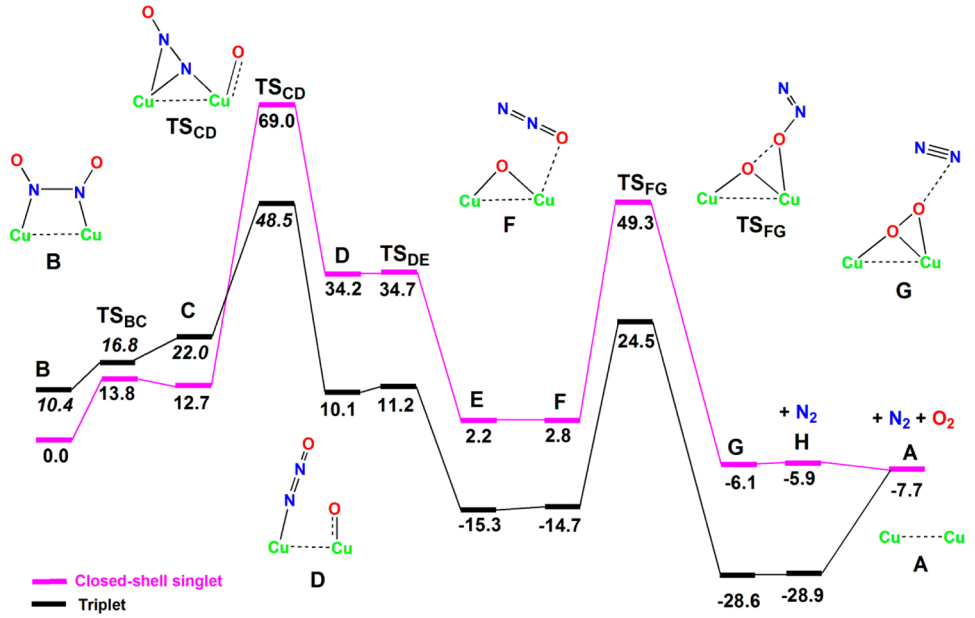

Figure 3. Calculated energy profile diagram for the proton-free NO decomposition reaction. The values in italics correspond to the single-point energy calculations. All the relative energies are in kcal/mol.

all the mechanistic pathways for the reaction with and without protons.

a. Mechanism of Proton-Free NO Decomposition Reaction over 1T Configuration. The intermediate and transition state structures proposed in the proton-free reaction mechanism are shown in Figure 2. Optimized geometries of the QM layer for all the structures are given in the Supporting Information. Figure 3 shows a calculated potential energy diagram for the catalytic reaction pathways. The initial zeolite complex with a dinuclear Cu structure is represented as **A**. As described above, the catalytic cycle begins with the N-down adsorption of two NO molecules on different Cu sites, resulting in the formation of a NO dimer (**B**). The adsorption energy for this process is calculated to be −34.3 kcal/mol. The N−N bond distance in **B** is 1.833 Å. Intermediate **B** is identified in the closed-shell singlet state. We also calculated the O-down conformation of the NO dimer, which is found to be 12.4 kcal/mol less stable than **B**. In the triplet or open-shell singlet spin state, the N−N bond formation over the active dinuclear Cu sites is unstable. Coordination of the oxygen atom of one of the two NO fragments on the active Cu(2) center leads to a side-on Cu(2)−NO species (**C**). This step is endothermic by 12.7 kcal/mol with an activation energy of 13.8 kcal/mol via transition state $\mathbf{TS_{BC}}$. In **C**, the N−N bond distance is decreased to 1.769 Å; thus the side-on NO binding would strengthen the N−N bond. As a result, the Cu(2)−O distance is shortened by 0.838 Å. From **C**, the nitrogen atom of side-on Cu(2)−NO inserts into the Cu(1)−NO bond via transition state $\mathbf{TS_{CD}}$ to form the insertion product **D**. The insertion barrier is calculated to be 56.3 kcal/mol, which is the highest activation barrier in the catalytic cycle. As a result of this step, the Cu(1)−N_2O bond is formed. Since **D** is more stable in the triplet state (energy difference between the two spin states is 24.1 kcal/mol), a spin change from the closed-shell singlet state to the triplet state is required. As a result of the spin-crossing, the formation of **D** is exothermic by 2.6 kcal/mol. Subsequent reactions are found to proceed on the triplet potential energy surface. We also noted that the open-shell singlet state is approximately 1−3 kcal/mol higher in energy than the corresponding triplet-state structures for all the intermediates.[20,40] In order to assess the oxidation states of the copper atoms in various intermediates, we calculated the Mulliken spin densities of all the steps in the triplet state, as summarized in Table 1. Calculated spin densities of **D** at the Cu(1), Cu(2), and O(2) atoms are 0.01, 0.47, and 1.38, respectively. The spin density of nearly zero on Cu(1) is reasonable for its oxidation state of +1. The total spin density of the Cu(2)O fragment is 1.85, suggesting the formal charges to be +2 and −1 for Cu(2) and O(2), respectively. Here, the O(2) atom is the spin carrier;[94] it forms a bridged coordination between the Cu atoms via transition state $\mathbf{TS_{DE}}$. A computed activation barrier for $\mathbf{TS_{DE}}$ is only 1.1 kcal/mol, indicating that this step can occur easily. In the transition state, the spin population of Cu(2) remains unchanged while there is a slight increase in the spin density of Cu(1) by 0.08. In **E**, the Cu(1)−N_2O bond distance is elongated to 4.474 Å. Calculated spin densities on Cu(1), Cu(2), and O(2) are 0.47, 0.61, and 0.70, respectively. However, if we count the formal charge of O(2) as −2, the oxidation states of both copper atoms would be +2.

Table 1. Calculated Spin Densities for Selected Atoms in the Proton-Free Mechanism in the Triplet State

species	Cu(1)	Cu(2)	N(1)	N(2)	O(1)	O(2)
D	0.01	0.47	0.05	−0.04	0.00	1.38
$\mathbf{TS_{DE}}$	0.09	0.47	0.04	−0.02	0.00	1.27
E	0.47	0.61	0.00	0.00	0.00	0.70
F	0.64	0.48	0.00	0.00	0.00	0.64
$\mathbf{TS_{FG}}$	0.62	0.48	−0.05	−0.04	0.02	0.73
G	0.51	0.31	0.00	0.00	0.43	0.56
H	0.51	0.31			0.44	0.56

The second part of the reaction is the decomposition of the N_2O molecule. Reassociation of N_2O to the Cu(2) active site of the Cu−O−Cu species results in the formation of **F**. The reunion of N_2O on Cu(2) causes an increase in the spin density value of Cu(1) from 0.47 to 0.64 while the spin density of

dx.doi.org/10.1021/cs500223z | ACS Catal. 2014, 4, 2075−2085

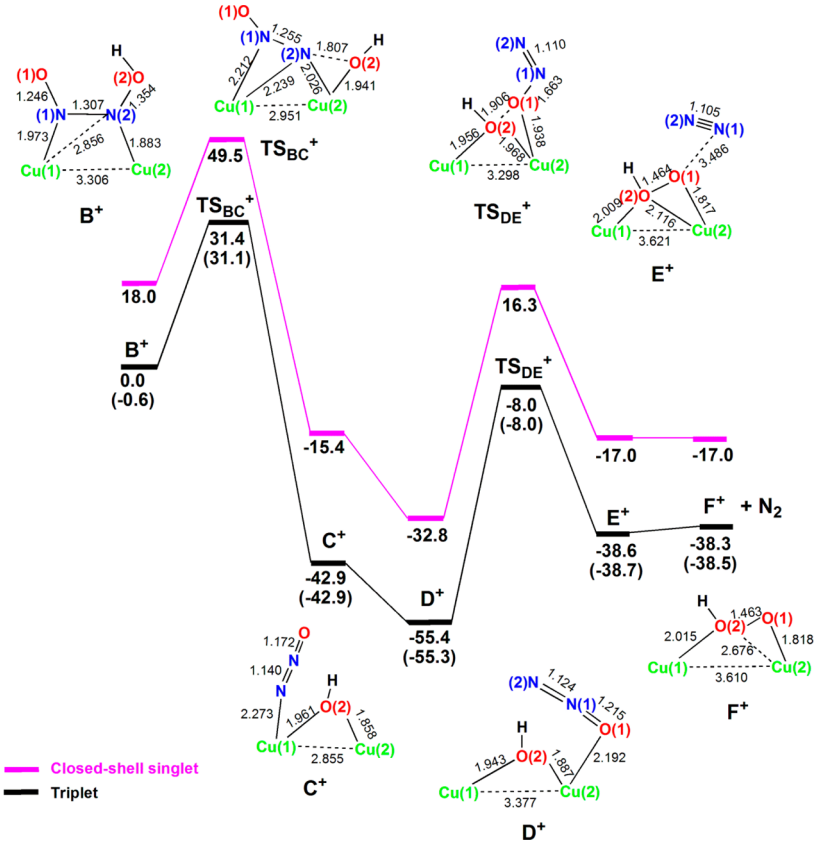

Figure 4. Energy profile diagram for the proton-assisted NO decomposition reaction. The values in parentheses are energies in the open-shell singlet state. All the relative energies are in kcal/mol, and distances are in Å.

Cu(2) decreases from 0.61 to 0.48. Upon proceeding from **F** to **G** via the transition state $\mathbf{TS_{FG}}$, O−O bond formation occurs, which results in the cleavage of the O−N_2 bond. This is a bent transition state with an NNO bond angle of 145.8°. The activation barrier for this step is 39.2 kcal/mol, and the process is exothermic by 13.9 kcal/mol. In $\mathbf{TS_{FG}}$, the O−O distance is shortened to 2.005 from 2.856 Å. This is reflected in the spin density values of O(1) and O(2). The intermediate thus formed is **G**, where the O−O bond is shortened by 0.629 from 2.005 Å. At the same time, the O−N_2 bond is elongated to 2.906 from 1.528 Å. In **G**, calculated spin densities of O(1) and O(2) are 0.43 and 0.56, respectively. The increase in the spin density of O(1) from 0.02 to 0.43 shows the formation of an O−O bond. The shorter O−O distance of 1.376 Å shows that the O_2 moiety exists mainly in the form of superoxide $(O-O)^-$ rather than peroxide $(O-O)^{2-}$. The spin density values of 0.51 and 0.31 at the Cu(1) and Cu(2) atoms in **G** indicate that the oxidation states of Cu(1) and Cu(2) are closer to +2 and +1, respectively. Desorption of N_2 yields **H** wherein one of the oxygen atoms in the O_2 molecule displays a bridging bond between the two Cu centers in a superoxide fashion with a puckered structure, which can be represented as [Cu−(μ-η^2:η^1-superoxo)−Cu]. The spin density values of **H** are nearly unchanged, and hence the oxidation states of the copper atoms remain the same as in **G**. The shorter bond length of Cu(2)−O(1) (1.869 Å) compared to Cu(1)−O(2) (1.903 Å) is also evident from the lower spin density value of the Cu(2) atom. O_2 can desorb from **H** with a desorption energy of 21.2 kcal/mol, and thus the active sites are regenerated (**A**). The entire catalytic reaction is exothermic by 7.7 kcal/mol.

b. Mechanism of Proton-Assisted NO Decomposition Reaction over 1T Configuration. In this section, we re-evaluate the NO decomposition mechanism upon the addition of one proton to the NO dimer adsorbed on the dicopper active sites. A computed energy profile diagram for the corresponding reaction is sketched in Figure 4. It may be noted that for all the intermediates and transition states, the triplet-state structures are more stable than the corresponding closed-shell singlet state structures. Thus, the discussion in the following section is based on the structures and energies corresponding to the triplet state. Mulliken spin density values for selected atoms are listed in Table 2. The open-shell singlet energy values are also comparable to the triplet-state energy values. As shown in eq 7, the reaction is initiated by N-down adsorption of both NO molecules on different Cu active sites. $\mathbf{B^+}$ shows a proton incorporated NO dimer over the active dicopper site (Figure 4). The N−N bond length in $\mathbf{B^+}$ is 1.307 Å, shorter by 0.526 Å compared to **B** in the proton-free

Table 2. Calculated Spin Densities for Selected Atoms in the Proton-Assisted Mechanism in the Triplet State

species	Cu(1)	Cu(2)	N(1)	N(2)	O(1)	O(2)
$\mathbf{B^+}$	0.53	0.64	−0.01	0.07	0.08	0.02
$\mathbf{TS_{BC}^+}$	0.38	0.58	−0.02	0.00	0.08	0.21
$\mathbf{C^+}$	0.62	0.64	0.01	0.00	0.03	0.16
$\mathbf{D^+}$	0.63	0.69	0.00	0.02	0.01	0.16
$\mathbf{TS_{DE}^+}$	0.62	0.66	0.00	−0.02	0.11	0.14
$\mathbf{E^+}$	0.60	0.56	0.00	0.00	0.25	0.04
$\mathbf{F^+}$	0.60	0.56			0.25	0.04

dx.doi.org/10.1021/cs500223z | ACS Catal. 2014, 4, 2075−2085

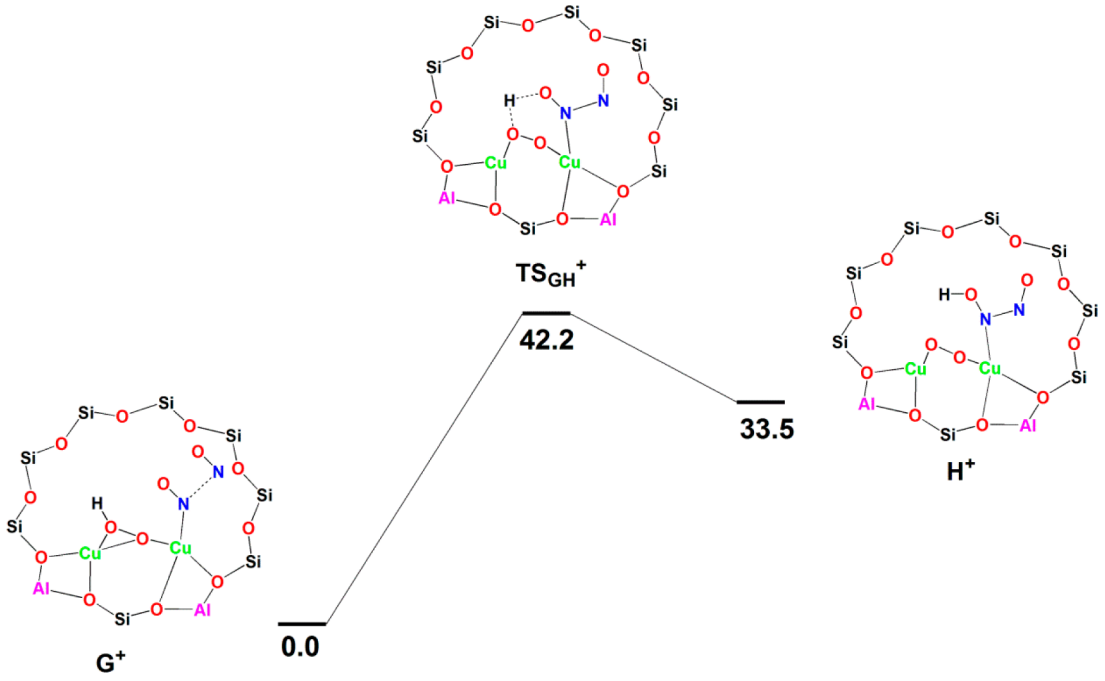

Figure 5. Energy profile diagram for the proton abstraction step with relative energies in the triplet (t) state. All the relative energies are in kcal/mol.

mechanism. The sum of the spin densities on the N(1), N(2), O(1), and O(2) atoms is 0.16 in $\mathbf{B}^+$, indicating a closed-shell configuration of N_2O_2 on the dicopper center with a formal charge of −2. This is also reflected by the shorter N−N and longer N−O distances of N_2O_2 when a proton is associated with it. Since the spin densities on Cu(1) and Cu(2) are 0.53 and 0.64, respectively, the oxidation states of Cu(1) and Cu(2) can be assigned to +2. Unlike the mechanism shown above, the intermediate with side-on binding of one of the NO fragments in the NO dimer is absent in the proton-assisted mechanism. Also, the transition state corresponding to $\mathbf{TS}_{DE}$ is not found. Then, a nitrogen atom of the Cu(2)N−OH$^+$ fragment inserts into the Cu(1)−NO bond through the transition state $\mathbf{TS}_{BC}^+$, leading to the insertion product $\mathbf{C}^+$. At $\mathbf{TS}_{BC}^+$, the N−OH$^+$ bond is elongated to 1.807 Å. In the transition state, the spin density on Cu(1) is decreased from 0.53 to 0.38, whereas a slight decrease from 0.64 to 0.58 is noted for Cu(2). As a result of this transition state, the Cu(1)−N_2O bond is formed, which is followed by the bridging of OH$^+$ between the two Cu active species ($\mathbf{C}^+$). This step is exothermic by 42.9 kcal/mol, and the energy barrier is 31.4 kcal/mol. The intermediate thus formed is in accordance with the earlier theoretical predictions by Sayle et al., who suggested that a copper cluster existing in the form of Cu−OH$^+$−Cu is a possible active site for the NO decomposition reaction.[95] In $\mathbf{C}^+$, spin densities of the Cu(1), Cu(2), and O(2) atoms are 0.62, 0.64, and 0.16, respectively, suggesting that the copper atoms exist in the +2 oxidation state while O(2) is nearly in the closed-shell state with the formal oxidation state of −2. The next step is the reorientation of N_2O and its further coordination to the active site Cu(2) with the O atom as a coordinating atom, leading to the formation of $\mathbf{D}^+$. This step is exothermic by 12.5 kcal/mol. The cleavage of the N_2−O bond followed by oxygen abstraction by the bridging Cu−OH$^+$−Cu group occurs via transition state $\mathbf{TS}_{DE}^+$, which results in the product $\mathbf{E}^+$. This step is endothermic by 16.8 kcal/mol and needs an activation barrier of 47.4 kcal/mol. The O−O bond formation is evident from an increase in the spin density value of O(1) from 0.01 to 0.11. The stability of the Cu−OH$^+$−Cu species is responsible for the larger activation barrier.[95,96] In $\mathbf{E}^+$, spin density values of O(1) and O(2) are 0.25 and 0.04, respectively, and a calculated O(1)−O(2) distance is 1.464 Å, suggesting that the dioxygen moiety exists in the hydroperoxide $(O-OH)^-$ form. Subsequently, an N_2 molecule can be eliminated from $\mathbf{F}^+$, and an O_2H^+ bridged dicopper species $[Cu-O_2H-Cu]^+$ ($\mathbf{F}^+$) is produced. In $\mathbf{F}^+$, the dioxygen bound to dicopper is in a bent μ-peroxo fashion with a Cu−Cu separation of 3.610 Å. The spin density values for all the atoms are nearly unchanged, and hence the two Cu atoms are in the formal oxidation state of +2.

To regenerate O_2, the proton attached on the dioxygen should be eliminated. This can be achieved through proton abstraction by the NO dimer from $\mathbf{F}^+$. The adsorption of the NO dimer over one of the Cu active sites of $\mathbf{F}^+$ leads to the formation of $\mathbf{G}^+$. The abstraction of the proton by ONNO occurs via transition state $\mathbf{TS}_{GH}^+$ in the triplet potential energy state. This process is endothermic by 33.5 kcal/mol with an activation barrier of 42.2 kcal/mol (Figure 5). Finally, O_2 can be desorbed from the dimeric active species $\mathbf{H}^+$, and the process is exothermic by 11.3 kcal/mol. The dioxygen free complex can isomerize to the initial reactant complex $\mathbf{B}^+$.

c. Comparison of Proton-Free and Proton-Assisted NO Decomposition Mechanisms over 1T. For a comparison of the relative energies of the transition states and intermediates involved in the proton-free and proton-assisted mechanisms, energy diagrams based on a common scale are required. It is possible that the interaction of NO with the protonic sites of zeolite framework results in the formation of HNO.[63,97] However, HNO is the protonated one-electron reduced form of NO, and hence it is unlikely to treat it as a reference for the common energy scale. In fact, the proton source is the acidic site of the zeolite framework; we therefore used a proton present in the acidic site of the small **5T** cluster model as a reference system. We also considered H_3O^+ as a reference system to understand how the choice of the reference

dx.doi.org/10.1021/cs500223z | ACS Catal. 2014, 4, 2075−2085

system influences the relative energies of various species involved in the proton-free as well as proto-assisted mechanisms. All these details along with the energy level diagrams shown in Figures 3, 4, and 5 based on these common scales are provided in the Supporting Information (Figures S1 and S2).

By comparing the energy diagrams of the proton-free and proton-assisted NO decomposition mechanisms, it is obvious that the activation energy for N_2O formation is considerably lowered when a proton is incorporated in the NO decomposition reaction. The activation energy needed for the production of N_2O in the proton-free mechanism is 24.9 kcal/mol more than the same reaction in the proton-assisted mechanism. This step is thermodynamically more favored in the proton-assisted mechanism. The presence of a proton on the NO dimer formed over the dinuclear active species will weaken the ONN−OH^+ bond. The N−O bond lengths in ONN−OH^+ and ONN−O attached to the dicopper centers are 1.354 and 1.172 Å, respectively. The weakening of the ONN−OH^+ bond strengthens the N−N bond of this species, which facilitates the formation of N_2O. Most of the theoretical studies predicted that the production of N_2O from NO is an energetically favorable process, which requires an activation barrier around 18−20 kcal/mol, while the decomposition of N_2O is the rate-limiting step with an activation energy value that would fall in the 38−43 kcal/mol range.[45,52,55] It may be noted that in most of the theoretical studies O-down adsorbed NO dimer on the single Cu active site was considered as the initial reactant complex, though the more favorable N-down adsorbed NO dimer exists over Cu species. The mechanistic studies depicted here showed that the production of N_2O from the N-down adsorbed NO dimer is energetically unfavorable in the absence of a proton.

Comparison of relative energy levels for the N_2O decomposition step in the proton-free and proton-assisted mechanisms showed that N_2O decomposition is more favored in the proton-free mechanism. In the proton-free mechanism this process is exothermic by 13.9 kcal/mol with an activation barrier of 39.2 kcal/mol, while in the proton-assisted mechanism the corresponding step is endothermic by 16.8 kcal/mol and needs to overcome a barrier of 47.4 kcal/mol. Although the dissociation of N_2O is a difficult step to have occur in the proton-assisted mechanism, this step cannot be ruled out since the reaction rate is higher at temperatures between 673 and 773 K. The proton abstraction from the Cu−O_2H^+−Cu species is also a difficult process since this step requires an activation barrier of 42.2 kcal/mol, and the process is endothermic by 33.5 kcal/mol. After the proton abstraction, O_2 can easily desorb from the resulting complex.

d. NO Decomposition on 2T and Its Comparison with 1T. The reaction path in the decomposition of NO over **2T** proceeds in a similar way as in the case of **1T**, although the Cu−Cu distance is 0.470 Å longer in **2T**. Detailed mechanistic features of the NO decomposition reaction with and without a proton over **2T** are given in the Supporting Information (Figures S9−S11). In the proton-free mechanism, the NO adsorption energy on **2T** is −41.0 kcal/mol, which is higher than that on **1T** by −6.7 kcal/mol. This result suggests that the NO dimer will be more stable on **2T** due to the lower electrostatic repulsion between the two Cu active sites. The activation energy barriers for various reaction steps over **2T** and **1T** are comparable. The barrier for the formation of side-on Cu−η^2-NO for one of the NO molecules on **2T** is 13.8 kcal/mol, which is almost the same as that of **1T**. The barrier for the rate-determining step, i.e., the formation of N_2O through the N insertion of one of the NO molecules into the Cu−NO, is 55.3 kcal/mol. The corresponding step on **1T** needed an activation barrier of 56.3 kcal/mol. The transition state leading to the decomposition of N_2O has been found to have an activation barrier of 42.3 kcal/mol, which is higher than that of **1T** by 3.1 kcal/mol.

When a proton is present on the NO dimer, the N−N bond distance is shortened by 0.567 Å. In the proton-assisted mechanism, an intermediate with side-on binding of the N−OH fragment of the NO dimer over a Cu active site is found. The activation barrier for the formation of N_2O is 17.3 kcal/mol, which is 14.1 kcal/mol lower than that of **1T**. The less electrostatic repulsion between the copper atoms is probably the reason for the further decrease in the activation barrier compared to **1T**. The decomposition of N_2O requires an activation barrier of 48.4 kcal/mol, which is 1.0 kcal/mol higher than that of **1T**. The proton transfer back to the two NO molecules from dioxygen is the final step of the catalytic cycle. The activation energy for this process is 34.3 kcal/mol, and the process is endothermic by 33.0 kcal/mol, whereas the proton transfer process on **1T** is endothermic by 33.5 kcal/mol with an energy barrier of 42.2 kcal/mol, indicating that the final step is more favorable on **2T**. In both the models, it is evident that the proton-assisted mechanism is in agreement with the experimental observations that N_2O decomposition and O_2 desorption are the rate-governing processes in the NO decomposition reaction. Conversely, the two models showed that N_2O decomposition is comparatively easy over the Cu−O−Cu unit present in Cu-ZSM-5. In the highly loaded Cu-ZSM-5, the presence of copper pairs in the form of Cu−O−Cu is supported by its characteristic CT band at 22 700 cm^{-1}.[10,11,21] However, no theoretical studies satisfactorily explained the role of these species in the NO decomposition mechanism. Our mechanistic studies clearly demonstrate that the Cu−O−Cu species is an active center for the decomposition of N_2O.

CONCLUSIONS

We explored the mechanism of the direct decomposition of NO over adjacent dimeric Cu active sites using QM/MM calculations to characterize the role of acidic proton in the catalytic pathways. The most favorable adsorption mode of N-down Cu−N(O)−N(O)−Cu species is considered as a starting reactant species in this study. As a generally accepted mechanism, two main steps in the decomposition reaction were taken into account: (i) production of N_2O and (ii) decomposition of N_2O into N_2 and O_2. Our mechanistic study showed that if a proton is absent, the rate-limiting step for the NO decomposition reaction is the production of N_2O, which requires an activation energy of 56.3 and 55.3 kcal/mol, respectively, for models **1T** and **2T**. However, when a proton is added in these catalytic cycles, the activation barrier is significantly reduced to 31.4 and 17.3 kcal/mol, respectively. The presence of protons strengthened the N−N bond of the NO dimer formed as an intermediate, which will facilitate the formation of N_2O. This is in agreement with the experimental observations that protonation plays a pivotal role in the formation of N_2O in the nitric oxide reductase (NOR) type reactions. The proton-assisted mechanism generates a stable intermediate Cu−OH^+−Cu, and further N_2O decomposition proceeds with a relatively high activation barrier of 47.4 and

dx.doi.org/10.1021/cs500223z | ACS Catal. 2014, 4, 2075−2085

48.4 kcal/mol, respectively, for **1T** and **2T**. The present study corroborates experimental findings that the Cu−O−Cu species present in the Cu-ZSM-5 system can facilitate the decomposition of N_2O.

■ ASSOCIATED CONTENT

Supporting Information

QM layer corresponding to the ONIOM optimized geometries of all the structures, energy profile diagrams computed using the single point energy calculations at the ONIOM (TPSSh/BS:UFF) as well as ONIOM (B3LYP*/BS:UFF) levels of theory, energy profile diagram based on a common scale, and energy profile diagram for the NO decomposition over **2T**. This material is available free of charge via the Internet at http://pubs.acs.org.

■ AUTHOR INFORMATION

Corresponding Author

*Tel: +81-92-802-2529. E-mail: kazunari@ms.ifoc.kyushu-u.ac.jp.

Notes

The authors declare no competing financial interest.

■ ACKNOWLEDGMENTS

We thank Grants-in-Aid for Scientific Research (Nos. 22245028, 24109014, and 24550190) from the Japan Society for the Promotion of Science (JSPS) and the Ministry of Education, Culture, Sports, Science and Technology of Japan (MEXT) and the MEXT Projects of "Integrated Research on Chemical Synthesis" and "Elements Strategy Initiative to Form Core Research Center."

■ REFERENCES

(1) Shelef, M. *Chem. Rev.* **1995**, *95*, 209−225.
(2) Iwamoto, M.; Furukawa, H.; Mine, Y.; Uemura, F.; Mikuriya, S.; Kagawa, S. *J. Chem. Soc., Chem. Commun.* **1986**, 1272−1273.
(3) Iwamoto, M.; Yahiro, H.; Tanda, K.; Mizuno, N.; Mine, Y.; Kagawa, S. *J. Phys. Chem.* **1991**, *95*, 3727−3730.
(4) Campa, M. C.; Indovina, V.; Minelli, G.; Moretti, G.; Pettiti, I.; Porta, P.; Riccio, A. *Catal. Lett.* **1994**, *23*, 141−149.
(5) Moretti, G.; Dossi, C.; Fusi, A.; Recchia, S.; Psaro, R. *Appl. Catal., B* **1999**, *20*, 67−73.
(6) Iwamoto, M.; Yahiro, H. *Catal. Today* **1994**, *22*, 5−18.
(7) Li, Y.; Hall, W. K. *J. Phys. Chem.* **1990**, *94*, 6145−6148.
(8) Kumashiro, R.; Kuroda, Y.; Nagao, M. *J. Phys. Chem. B* **1999**, *103*, 89−96.
(9) Vanelderen, P.; Hadt, R. G.; Smeets, P. J.; Solomon, E. I.; Schoonheydt, R. A.; Sels, B. F. *J. Catal.* **2011**, *284*, 157−164.
(10) Groothaert, M. H.; van Bokhoven, J. A.; Battiston, A. A.; Weckhuysen, B. M.; Schoonheydt, R. A. *J. Am. Chem. Soc.* **2003**, *125*, 7629−7640.
(11) Smeets, P. J.; Groothaert, M. H.; van Teeffelen, R. M.; Leeman, H.; Hensen, E. J. M.; Schoonheydt, R. A. *J. Catal.* **2007**, *245*, 358−368.
(12) Smeets, P. J.; Sels, B. F.; van Teeffelen, R. M.; Leeman, H.; Hensen, E. J. M.; Schoonheydt, R. A. *J. Catal.* **2008**, *256*, 183−191.
(13) Li, Y.; Hall, W. K. *J. Catal.* **1991**, *129*, 202−215.
(14) Jang, H.-J.; Hall, W. K.; d'Itri, J. L. *J. Phys. Chem.* **1996**, *100*, 9416−9420.
(15) Valyon, J.; Hall, W. K. *Catal. Lett.* **1993**, *19*, 109−119.
(16) Moretti, G. *Catal. Lett.* **1994**, *23*, 135−140.
(17) Moretti, G. *Catal. Lett.* **1994**, *28*, 143−152.
(18) Turnes Palomino, G.; Fisicaro, P.; Bordiga, S.; Zecchina, A.; Giamello, E.; Lamberti, C. *J. Phys. Chem. B* **2000**, *104*, 4064−4073.
(19) Goodman, B. R.; Schneider, W. F.; Hass, K. C.; Adams, J. B. *Catal. Lett.* **1998**, *56*, 183−188.
(20) Goodman, B. R.; Hass, K. C.; Schneider, W. F.; Adams, J. B. *J. Phys. Chem. B* **1999**, *103*, 10452−10460.
(21) Vanelderen, P.; Vancauwenbergh, J.; Sels, B. F.; Schoonheydt, R. A. *Coord. Chem. Rev.* **2013**, *257*, 483−494.
(22) Groothaert, M. H.; Lievens, K.; Leeman, H.; Weckhuysen, B. M.; Schoonheydt, R. A. *J. Catal.* **2003**, *220*, 500−512.
(23) Groothaert, M. H.; Lievens, K.; van Bokhoven, J. A.; Battiston, A. A.; Weckhuysen, B. M.; Pierloot, K.; Schoonheydt, R. A. *Stud. Surf. Sci. Catal.* **2004**, *154*, 2449−2457.
(24) Da Costa, P.; Moden, B.; Meitzner, G. D.; Lee, D. K.; Iglesia, E. *Phys. Chem. Chem. Phys.* **2002**, *4*, 4590−4601.
(25) Eichler, U.; Kölmel, C. M.; Sauer, J. *J. Comput. Chem.* **1997**, *18*, 463−477.
(26) Becke, A. D. *J. Chem. Phys.* **1993**, *98*, 5648−5652.
(27) Spuhler, P.; Holthausen, M. C.; Nachtigallova, D.; Nachtigall, P.; Sauer, J. *Chem.—Eur. J.* **2002**, *8*, 2099−2115.
(28) Spoto, G.; Zecchina, A.; Bordiga, S.; Ricchiardi, G.; Martra, G.; Leofanti, G.; Petrini, G. *Appl. Catal. B: Environ.* **1994**, *3*, 151−172.
(29) Lamberti, C.; Bordiga, S.; Salvalaggio, M.; Spoto, G.; Zecchina, A.; Geobaldo, F.; Vlaic, G.; Bellatreccia, M. *J. Phys. Chem. B* **1997**, *101*, 344−360.
(30) Itadani, A.; Tanaka, M.; Mori, T.; Nagao, M.; Kobayashi, H.; Kuroda, Y. *J. Phys. Chem. C* **2007**, *111*, 12011−12023.
(31) Spoto, G.; Bordiga, S.; Scarano, D.; Zecchina, A. *Catal. Lett.* **1992**, *13*, 39−44.
(32) Dědeček, J.; Wichterlová, B. *Phys. Chem. Chem. Phys.* **1999**, *1*, 629−637.
(33) Itadani, A.; Sugiyama, H.; Tanaka, M.; Mori, T.; Nagao, M.; Kuroda, Y. *J. Phys. Chem. C* **2007**, *111*, 16701−16705.
(34) Anpo, M.; Matsuoka, M.; Shioya, Y.; Yamashita, H.; Giamello, E.; Morterra, C.; Che, M.; Patterson, H. H.; Webber, S.; Ouellette, S.; Fox, M. A. *J. Phys. Chem.* **1994**, *98*, 5744−5750.
(35) Lisi, L.; Pirone, R.; Russo, G.; Santamaria, N.; Stanzione, V. *Appl. Catal., A* **2012**, *413−414*, 117−131.
(36) Yamashita, H.; Matsuoka, M.; Tsuji, K.; Shioya, Y.; Anpo, M.; Che, M. *J. Phys. Chem.* **1996**, *100*, 397−402.
(37) Hamada, H.; Matsubayashi, N.; Shimada, H.; Kintaichi, Y.; Ito, T.; Nishijima, A. *Catal. Lett.* **1990**, *5*, 189−196.
(38) Deka, U.; Lezcano-Gonzalez, I.; Weckhuysen, B. M.; Beale, A. M. *ACS Catal.* **2013**, *3*, 413−427.
(39) Yumura, T.; Takeuchi, M.; Kobayashi, H.; Kuroda, Y. *Inorg. Chem.* **2009**, *48*, 508−517.
(40) Woertink, J. S.; Smeets, P. J.; Groothaert, M. H.; Vance, M. A.; Sels, B. F.; Schoonheydt, R. A.; Solomon, E. I. *Proc. Natl. Acad. Sci. U.S.A.* **2009**, *106*, 18908−18913.
(41) Pidko, E. A.; Hensen, E. J. M.; van Santen, R. A. *Proc. R. Soc. A* **2012**, *468*, 2070−2086.
(42) Giamello, E.; Murphy, D.; Magnacca, G.; Morterra, C.; Shioya, Y.; Nomura, T.; Anpo, M. *J. Catal.* **1992**, *136*, 510−520.
(43) Aylor, A. W.; Larsen, S. C.; Reimer, J. A.; Bell, A. T. *J. Catal.* **1995**, *157*, 592−602.
(44) Iwamoto, M.; Hamada, H. *Catal. Today* **1991**, *10*, 57−71.
(45) Schneider, W. F.; Hass, K. C.; Ramprasad, R.; Adams, J. B. *J. Phys. Chem. B* **1998**, *102*, 3692−3705.
(46) Trout, B. L.; Chakraborty, A. K.; Bell, A. T. *J. Phys. Chem.* **1996**, *100*, 17582−17592.
(47) Bell, A. T. *Catal. Today* **1997**, *38*, 151−156.
(48) Schneider, W. F.; Hass, K. C.; Ramprasad, R.; Adams, J. B. *J. Phys. Chem. B* **1997**, *101*, 4353−4357.
(49) Yokomichi, Y.; Ohtsuka, H.; Tabata, T.; Okada, O.; Yokoi, Y.; Ishikawa, H.; Yamaguchi, R.; Matsui, H.; Tachibana, A.; Yamabe, T. *Catal. Today* **1995**, *23*, 431−437.
(50) Solans-Monfort, X.; Sodupe, M.; Branchadell, V. *Chem. Phys. Lett.* **2003**, *368*, 242−246.
(51) Ramprasad, R.; Hass, K. C.; Schneider, W. F.; Adams, J. B. *J. Phys. Chem. B* **1997**, *101*, 6903−6913.
(52) Tajima, N.; Hashimoto, M.; Toyama, F.; El-Nahas, A. M.; Hirao, K. *Phys. Chem. Chem. Phys.* **1999**, *1*, 3823−3830.

(53) Solans-Monfort, X.; Branchadell, V.; Sodupe, M. *J. Phys. Chem. B* **2002**, *106*, 1372−1379.
(54) Izquierdo, R.; Rodríguez, L. J.; Añez, R.; Sierraalta, A. *J. Mol. Catal. A: Chem.* **2011**, *348*, 55−62.
(55) Morpurgo, S.; Moretti, G.; Bossa, M. *J. Mol. Catal. A: Chem.* **2012**, *358*, 134−144.
(56) Zakharov, I. I.; Ismagilov, Z. R.; Ruzankin, S. Ph.; Anufrienko, V. F.; Yashnik, S. A.; Zakharova, O. I. *J. Phys. Chem. C* **2007**, *111*, 3080−3089.
(57) Kuroda, Y.; Iwamoto, M. *Top. Catal* **2004**, *28*, 111−118.
(58) Arikawa, Y.; Asayama, T.; Moriguchi, Y.; Agari, S.; Onishi, M. *J. Am. Chem. Soc.* **2007**, *129*, 14160−14161.
(59) Arikawa, Y.; Matsumoto, N.; Asayama, T.; Umakoshi, K.; Onishi, M. *Dalton Trans.* **2011**, *40*, 2148−2150.
(60) Arikawa, Y.; Onishi, M. *Coord. Chem. Rev.* **2012**, *256*, 468−478.
(61) van Santen, R. A. *Stud. Surf. Sci. Catal.* **1994**, *85*, 273−294.
(62) Li, J.; Li, S. *Phys. Chem. Chem. Phys.* **2007**, *9*, 3304−3311.
(63) Kobayashi, H.; Ohkubo, K. *Appl. Surf. Sci.* **1997**, *121/122*, 111−115.
(64) Shiota, Y.; Suzuki, K.; Yoshizawa, K. *Organometallics* **2006**, *25*, 3118−3123.
(65) Maseras, F.; Morokuma, K. *J. Comput. Chem.* **1995**, *16*, 1170−1179.
(66) Humbel, S.; Sieber, S.; Morokuma, K. *J. Chem. Phys.* **1996**, *105*, 1959−1967.
(67) Wattanakit, C.; Nokbin, S.; Boekfa, B.; Pantu, P.; Limtrakul, J. *J. Phys. Chem. C* **2012**, *116*, 5654−5663.
(68) Mosallanejad, S.; Dlugogorski, B. Z.; Kennedy, E. M.; Stockenhuber, M. *J. Phys. Chem. C* **2013**, *117*, 19365−19372.
(69) Kumsapaya, C.; Bobuatong, K.; Khongpracha, P.; Tantirungrotechai, Y.; Limtrakul, J. *J. Phys. Chem. C* **2009**, *113*, 16128−16137.
(70) Jungsuttiwong, S.; Lomratsiri, J.; Limtrakul, J. *Int. J. Quantum Chem.* **2011**, *111*, 2275−2282.
(71) Frisch, M. J.; Trucks, G. W.; Schlegel, H. B.; Scuseria, G. E.; Robb, M. A.; Cheeseman, J. R.; Scalmani, G.; Barone, V.; Mennucci, B.; Petersson, G. A.; Nakatsuji, H.; Caricato, M.; Li, X.; Hratchian, H. P.; Izmaylov, A. F.; Bloino, J.; Zheng, G.; Sonnenberg, J. L.; Hada, M.; Ehara, M.; Toyota, K.; Fukuda, R.; Hasegawa, J.; Ishida, M.; Nakajima, T.; Honda, Y.; Kitao, O.; Nakai, H.; Vreven, T.; Montgomery, J. A., Jr.; Peralta, J. E.; Ogliaro, F.; Bearpark, M.; Heyd, J. J.; Brothers, E.; Kudin, K. N.; Staroverov, V. N.; Keith, T.; Kobayashi, R.; Normand, J.; Raghavachari, K.; Rendell, A.; Burant, J. C.; Iyengar, S. S.; Tomasi, J.; Cossi, M.; Rega, N.; Millam, J. M.; Klene, M.; Knox, J. E.; Cross, J. B.; Bakken, V.; Adamo, C.; Jaramillo, J.; Gomperts, R.; Stratmann, R. E.; Yazyev, O.; Austin, A. J.; Cammi, R.; Pomelli, C.; Ochterski, J. W.; Martin, R. L.; Morokuma, K.; Zakrzewski, V. G.; Voth, G. A.; Salvador, P.; Dannenberg, J. J.; Dapprich, S.; Daniels, A. D.; Farkas, O.; Foresman, J. B.; Ortiz, J. V.; Cioslowski, J.; Fox, D. J. *Gaussian 09*, Revision C.01; Gaussian, Inc.: Wallingford, CT, 2010.
(72) Vreven, T.; Morokuma, K.; Farkas, O.; Schlegel, H. B.; Frisch, M. J. *J. Comput. Chem.* **2003**, *24*, 760−769.
(73) Lee, C.; Yang, W.; Parr, R. G. *Phys. Rev. B* **1988**, *37*, 785−789.
(74) Wachters, A. J. H. *J. Chem. Phys.* **1970**, *52*, 1033−1036.
(75) Hay, P. J. *J. Chem. Phys.* **1977**, *66*, 4377−4384.
(76) Rappé, A. K.; Casewit, C. J.; Colwell, K. S.; Goddard, W. A., III; Skiff, W. M. *J. Am. Chem. Soc.* **1992**, *114*, 10024−10035.
(77) Meeprasert, J.; Jungsuttiwong, S.; Truong, T. N.; Namuangruk, S. *J. Mol. Graphics Modell.* **2013**, *43*, 31−40.
(78) Nie, X.; Janik, M. J.; Guo, X.; Song, C. *Phys. Chem. Chem. Phys.* **2012**, *14*, 16644−16653.
(79) Pantu, P.; Pabchanda, S.; Limtrakul, J. *Chem. Phys. Chem.* **2004**, *5*, 1901−1906.
(80) Nie, X.; Janik, M. J.; Guo, X.; Song, C. S. *J. Phys. Chem. C* **2012**, *116*, 4071−4082.
(81) Bobuatong, K.; Limtrakul, J. *Appl. Catal., A* **2003**, *253*, 49−64.
(82) Kasuriya, S.; Namuangruk, S.; Treesukol, P.; Tirtowidjojo, M.; Limtrakul, J. *J. Catal.* **2003**, *219*, 320−328.
(83) Rozanska, X.; van Santen, R. A.; Hutschka, F.; Hafner, J. *J. Am. Chem. Soc.* **2001**, *123*, 7655−7667.
(84) Clark, L. A.; Sierka, M.; Sauer, J. *J. Am. Chem. Soc.* **2003**, *125*, 2136−2141.
(85) Sun, Y.-X.; Yang, J.; Zhao, L.-F.; Dai, J.-X.; Sun, H. *J. Phys. Chem. C* **2010**, *114*, 5975−5984.
(86) Reiher, M.; Salomon, O.; Hess, B. A. *Theor. Chem. Acc.* **2001**, *107*, 48−55.
(87) Salomon, O.; Reiher, M.; Hess, B. A. *J. Chem. Phys.* **2002**, *117*, 4729−4737.
(88) Tao, J.; Perdew, J. P.; Staroverov, V. N.; Scuseria, G. E. *Phys. Rev. Lett.* **2003**, *91*, 146401−146404.
(89) Database of Zeolite Structures. http://www.iza-structure.org/databases/.
(90) Maihom, T.; Wannakao, S.; Boekfa, B.; Limtrakul, J. *Chem. Phys. Lett.* **2013**, *556*, 217−224.
(91) Gleeson, D. *J. Comput.-Aided Mol. Des.* **2008**, *22*, 579−585.
(92) Grunert, W.; Hayes, N. W.; Joyner, R. W.; Shpiro, E. S.; Siddiqui, M. R. H.; Baeva, G. N. *J. Phys. Chem.* **1994**, *98*, 10832−10846.
(93) Huang, Y.-J.; Wang, H. P.; Lee, J.-F. *Chemosphere* **1999**, *39*, 1347−1356.
(94) Shiota, Y.; Juhász, G.; Yoshizawa, K. *Inorg. Chem.* **2013**, *52*, 7907−7917.
(95) Sayle, D. C.; Catlow, C. R. A.; Gale, J. D.; Perrin, M. A.; Nortier, P. *J. Phys. Chem. A* **1997**, *101*, 3331−3337.
(96) Sayle, D. C.; Catlow, C. R. A.; Gale, J. D.; Perrin, M. A.; Nortier, P. *J. Mater. Chem.* **1997**, *7*, 1635−1639.
(97) Szanyi, J.; Paffett, M. T. *J. Catal.* **1996**, *164*, 232−245.